frontiers | Frontiers in Physics

ORIGINAL RESEARCH
published: 25 April 2022
doi: 10.3389/fphy.2022.833426

Diffusion and Synchronization Dynamics Reveal the Multi-Scale Patterns of Spatial Segregation

Aleix Bassolas, Sergio Gómez and Alex Arenas*

Departament d'Enginyeria Informàtica i Matemàtiques, Universitat Rovira i Virgili, Tarragona, Spain

Urban systems are characterized by populations with heterogeneous characteristics, and whose spatial distribution is crucial to understand inequalities in life expectancy or education level. Traditional studies on spatial segregation indicators focus often on first-neighbour correlations but fail to capture complex multi-scale patterns. In this work, we aim at characterizing the spatial distribution heterogeneity of socioeconomic features through diffusion and synchronization dynamics. In particular, we use the time needed to reach the synchronization as a proxy for the spatial heterogeneity of a socioeconomic feature, as for example, the income. Our analysis for 16 income categories in cities from the United States reveals that the spatial distribution of the most deprived and affluent citizens leads to higher diffusion and synchronization times. By measuring the time needed for a neighborhood to reach the global phase we are able to detect those that suffer from a steeper segregation. Overall, the present manuscript exemplifies how diffusion and synchronization dynamics can be used to assess the heterogeneity in the presence of node information.

Keywords: urban segregation, spatial heterogeneity, synchronization, phase-oscillators, diffusion

OPEN ACCESS

Edited by:
Haroldo V. Ribeiro,
State University of Maringá, Brazil

Reviewed by:
Zoltan Neda,
Babeş-Bolyai University, Romania
Matjaž Perc,
University of Maribor, Slovenia

****Correspondence:***
Aleix Bassolas
aleix.bassolas@gmail.com

Specialty section:
This article was submitted to Social Physics, a section of the journal Frontiers in Physics

Received: *11 December 2021*
Accepted: *04 April 2022*
Published: *25 April 2022*

Citation:
Bassolas A, Gómez S and Arenas A (2022) Diffusion and Synchronization Dynamics Reveal the Multi-Scale Patterns of Spatial Segregation. Front. Phys. 10:833426. doi: 10.3389/fphy.2022.833426

1 INTRODUCTION

The expansion of urbanization and progressive increase of the population in cities has intensified the concern over the many dimensions of segregation—i.e., school, economic or ethnics—that have a tangible impact in the health, education and equal opportunities of citizens [1–8]. In fact, quantifying the extent of segregation and the identification of economically and socially isolated neighborhoods has been a topic of wide interest that first led to the development of global metrics, and which were later extended to spatial metrics [9–14]. Most of the initial spatial measures were limited to first neighbour indices, which facilitated the development of multi-scalar indices that provide a more nuanced picture of segregation [15–21], yet understanding the role played by each of the scales and their interplay still remains a challenge.

Dynamical processes in general, and in particular diffusion [22–30] and synchronization [31–35] dynamics, have been widely studied in complex networks on account of their relation with the spread of diseases and information [36, 37] and real-world phenomena in social or economic systems [38–40]. Interestingly, they provide insights on the topological scales and structure of networks and reveal the existence of functional meso-scale structures [27, 30, 32, 34, 41].

Here we use previous knowledge on diffusion and synchronization dynamics to assess the multi-scale patterns of residential segregation. By moving the focus from the network topology and organization to the node states, we are able to measure how well distributed a population with a certain characteristic is using the time needed to reach the absorbing state. Our framework requires

thus the implementation of a population dynamic to drive the system towards the homogeneous state, in our case diffusion and synchronization dynamics. None of them constitute here an attempt to model or predict the changes in the spatial distribution of a population characteristic but are highly stylized simplifications of their evolution that allow us to measure the time needed to attain the homogeneous state, which we consider to be the non-segregated scenario. Dynamical approaches are thus introduced here not because they provide a realistic approximation to the evolution of population dynamics but because they offer a significant advantage to measure multi-scale correlations as they do not require to take distance explicitly into account. Moreover, the assumption that cities converge towards uniformity is rather unrealistic without a heavy external driver, and is only a means to construct our measures.

As case studies we provide an analysis on the distribution of citizens of a certain income category in cities from the United States, and the distribution of a set of socioeconomic indicators in the city of Paris throughout an average day (see **Supplementary Material Section 2** and **Supplementary Figures S8–S10**). The analysis on the spatial organization of income categories reveals that the most deprived and affluent sectors display higher diffusion and synchronization times linked to a higher heterogeneity, and allow us to split the cities in two groups depending on the difference on the level of segregation. Finally, we evaluate the level of synchronization at the neighborhood level which allow us to spot the more sensitive places in a city.

2 RESULTS

2.1 Diffusion Dynamics and Income Segregation

Citizens exhibit a huge diversity of characteristics usually captured by socioeconomic indicators such as education level, income or ethnicity, and they are often heterogeneously distributed in space: those individuals with similar characteristics tend to live close between them. To assess the heterogeneity of a population with a characteristic $k \in K$, we consider a graph $G(V, E)$ with adjacency matrix $A = \{a_{ij}\}$ in which the spatial units are represented as a set of nodes V connected by a set of edges E. The adjacency matrix A we have considered takes $a_{ij} = 1$ when spatial units i and j are adjacent and $a_{ij} = 0$ otherwise, which is the traditional connectivity matrix used to capture residential segregation. Still, other types of (weighted) matrices could be considered to assess, for example, the impact of mobility in segregation. The state of a node x_i^k is given by the fraction of citizens living in node i that belong to socioeconomic category (or class) k, written as

$$x_i^k = \frac{n_i^k}{\sum_{k'} n_i^{k'}}, \tag{1}$$

where n_i^k is the total number of citizens in unit i that belong to category k. As extreme cases, $x_i^k = 0$ when there are no citizens of category k living in i, and $x_i^k = 1$ when all the citizens in node i belong to category k. Of course, the normalization condition

$$\sum_{k \in K} x_i^k = 1 \tag{2}$$

is fulfilled for all nodes i.

TABLE 1 | Income range (in US dollars) corresponding to each category (or class).

Class	Income ($)
1	Less than 10,000
2	10,000–14,999
3	15,000–19,999
4	20,000–24,999
5	25,000–29,999
6	30,000–34,999
7	35,000–39,999
8	40,000–44,999
9	45,000–49,999
10	50,000–59,999
11	60,000–74,999
12	75,000–99,999
13	100,000–124,999
14	125,000–149,999
15	150,000–199,999
16	200,000 or more

To measure the multi-scalar patterns of segregation, our assumption is that cities suffering from stronger residential segregation are further from the stationary state where the citizens of category k are homogeneously distributed in space. Although cities are in continuous change and most likely far from equilibrium, similar approaches such as the long-standing Schelling and the Alonso-Muth-Mills models have been able to draw relevant conclusions from the equilibrium state [42, 43].

By adopting diffusion dynamics we do not refuse the high complexity of population dynamics influenced by a wide variety of demographic, economic, political, and behavioral factors [44–47] but avoid introducing further parameters and factors that could hinder our aim of characterizing the segregation of a particular population category. Bear in mind that our final goal is by no means to assess real-world migration processes but to construct a multi-scalar measure of segregation that does not explicitly include the distance and the use of more complex and realistic approaches that would complicate the interpretation of the results. Diffusion constitutes one of the most basic approximations to how information, or any other characteristic, is transmitted through a system. Although far from the real behavior, it provides one of the simplest scenarios where the flow of population follows a gradient.

In fact, we focus on one of the best-case scenarios where the values of x_i^k converge towards equilibrium following a gradient, which could be interpreted as the change of residence of citizens of category k to regions where they are less abundant.

We focus on the economic segregation in the metropolitan areas of the United States with more than 1 million inhabitants and analyze a dataset containing the number of households within an income interval k residing in each census tract (see **Table 1**).

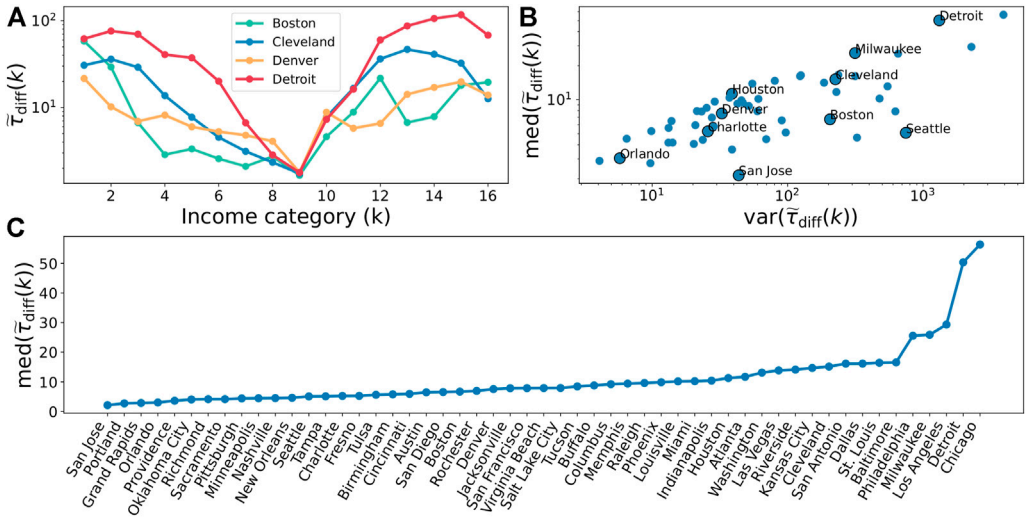

FIGURE 1 | Diffusion dynamics as a measure for income segregation. **(A)** Synchronization time for each of the 16 income categories in Boston, Cleveland, Denver and Detroit. **(B)** Median value of $\tilde{\tau}_{\text{diff}}(k)$ across income categories as a function of its variance. **(C)** Ranking for the median value of $\tilde{\tau}_{\text{diff}}(k)$ for the studied set of US cities.

Once we have the set of initial node states x_i^k, their evolution through time is determined by the diffusion dynamics

$$\frac{dx_i^k}{dt} = \frac{1}{s_i}\sum_{j=1}^{N} a_{ij}\left(x_j^k - x_i^k\right), \tag{3}$$

where

$$s_i = \sum_{j=1}^{N} a_{ij} \tag{4}$$

is the degree of node i. For simplification purposes, we have opted to use a normalized diffusion dynamic, with diffusion strength equal to 1. Note that we have independent diffusion processes for each category k.

The diffusion dynamic lasts until the stationary state, $x_i^k = x^k$, $\forall i$ is reached, and we denote the spanned time as $\tau_{\text{diff}}(k)$. Since the time to reach the stationary state can be infinitely large, we have considered that it is reached when the variance of x_i^k, in time, becomes lower than 0.0001. We hypothesize that lower values of $\tau_{\text{diff}}(k)$ are related to a more homogeneous distribution of the population within a category k, and the other way around when it is higher. In the extreme case in which all units have the same initial value of x_i^k, the diffusion time $\tau_{\text{diff}}(k)$ would attain its minimum value. As we aim to compare cities with different characteristics, we control for confounding factors such as the particular distribution of x^k or the topology of the graph by running the same diffusion dynamics on the same graph but where the values of x^k have been reshuffled, thus defining the average null-model diffusion time $\tau_{\text{diff}}^{\text{null}}(k)$ calculated over 500 reshuffling realizations. The relative diffusion time we will use throughout this manuscript can then be written as

$$\tilde{\tau}_{\text{diff}}(k) = \frac{\tau_{\text{diff}}(k)}{\tau_{\text{diff}}^{\text{null}}(k)}. \tag{5}$$

A relative diffusion time equal to one means that it is compatible with the null model, i.e., there are no remarkable spatial dependencies, while a greater value suggests that spatial heterogeneities delay the arrival to the stationary state.

We analyze the normalized diffusion times $\tilde{\tau}_{\text{diff}}(k)$ by running simulations for all US cities above 1 million of inhabitants and each of the 16 income categories k as a proxy for how heterogeneously distributed is the population; we have excluded New York City, whose adjacency network does not provide an accurate picture of residential segregation due to the particular geography of Manhattan. In **Figure 1A** we display $\tilde{\tau}_{\text{diff}}(k)$ in Boston, Cleveland, Detroit and Denver observing a common qualitative behavior: smaller values for middle-income categories, and higher ones for the categories in the extremes of the income distribution. Our results suggest that the wealthier and most deprived citizens suffer from stronger segregation and display a more clustered spatial distribution. More interestingly, category 9 seems to be the more homogeneously distributed across space, in agreement with the results observed in [20] and with the mean and standard deviation of x^k as well as the Moran's I (see **Supplementary Material Section 1** and **Supplementary Figure S1**). Still, there are strong quantitative differences, with Cleveland and Detroit displaying higher values for most of the categories, in contrast to Boston and Denver.

Since $\tilde{\tau}_{\text{diff}}(k)$ takes a set of 16 values for each city, we calculate their median and variance values over all categories to ease the comparison between the set of cities studied. While the median value provides information on the segregation across all economic categories, its variance reports the variability among them. **Figure 1B** shows this median value of $\tilde{\tau}_{\text{diff}}(k)$, $\text{med}\left(\tilde{\tau}_{\text{diff}}(k)\right)$ as a function of its variance, $\text{var}\left(\tilde{\tau}_{\text{diff}}(k)\right)$. The prior cities appear ordered as Detroit, Cleveland, Boston and Denver, although the variance is very similar for Cleveland and Boston, likely due to the high values observed for low-income categories in Boston. Finally, we provide in **Figure 1C** the ranking

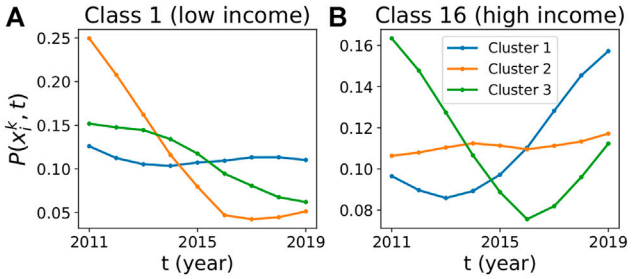

FIGURE 2 | Average temporal evolution of the abundance of households within the lowest and highest income. Temporal evolution of centroids after performing a k-means clustering on the normalized abundance of households with category k, $P(x_i^k, t)$, as a function of time t for the lower **(A)** and higher **(B)** income categories.

of the selected US cities according to med$(\tilde{\tau}_{\text{diff}}(k))$, as a measure of the overall segregation in cities. On top of it, we find cities such as Milwaukee or Detroit, which have been reported to suffer from economic and ethnic segregation [49–51].

By applying diffusion dynamics we implicitly assume that x^k evolves homogeneously towards consensus, which more than a realistic scenario, it is a means to calculate the time needed to reach consensus and obtain a measure of segregation. To further inspect the actual change of x_i^k between 2011 and 2019 in each of the spatial units i, we first construct the normalized time-series for each spatial unit across those years as

$$P\left(x_i^k, t\right) = \frac{x_i^k(t)}{\sum_{t'} x_i^k(t')}, \tag{6}$$

and then cluster, for each category k, the temporal profiles of all the nodes. For the clustering, we have made use of the k-means algorithm [52, 53], grouping together those units with a similar temporal evolution, and setting the number of clusters to 3. The resulting time-series of the corresponding centroids for the highest and lowest income categories are depicted in **Figure 2**, where a non-monotonic behavior is observed in most of the cases, with oscillatory behaviors through time of varying amplitude.

2.2 Synchronization Dynamics and Income Segregation

According to the oscillations in the temporal evolution of x_i^k (**Figure 2**), diffusion dynamics appear to be a rather simplistic approach to assess the time needed to converge. Even thought we do not aim to mimic the real evolution of x_i^k, we seek for a dynamic that at least can resemble its real behaviour in a qualitative way. Thus, despite still constituting a stylized approximation, a dynamical process with an oscillatory behavior, like a system of coupled Kuramoto oscillators, appears to be a better way to assess the spatial heterogeneity of socioeconomic indicators across cities. To analyze segregation in terms of synchronization dynamics, we treat each of the spatial units i as an individual Kuramoto oscillator, with an initial phase $\theta_i^k(0)$ that is set by distributing the fraction of population in node i that belongs to a category k within the range $[0, \pi]$ as

$$\theta_i^k(0) = x_i^k \pi. \tag{7}$$

The interaction between spatial units is given by the Kuramoto model

$$\dot{\theta}_i^k(t) = \omega_i^k + \frac{1}{s_i}\sum_{j=1}^{N} a_{ij} \sin\left(\frac{\theta_j^k(t) - \theta_i^k(t)}{2}\right), \tag{8}$$

where we have modified the traditional interaction term between oscillators by dividing the angle difference by two, allowing for the interaction between regions displaying extreme values of x_i^k. Additionally, to facilitate the global synchronization of the system, we set all the individual natural frequencies of the oscillators to the same value, i.e., $\omega_i = 1$, $\forall i$. In order to account separately the segregation of each category k, our approach assumes that there is no interaction between categories and, thus, x_i^k synchronize independently of k.

We use the standard order parameter $|z^k|$ to assess the global level of synchronization for a category k in a city, where

$$z^k = \frac{1}{N}\sum_{j=1}^{N} e^{i\theta_j^k}, \tag{9}$$

and N is the total number of spatial units or Kuramoto oscillators [35]. We consider that a city has reached the synchronized state when $|z^k| > 0.999$. As in the case of diffusion, we assess how the distribution of initial phases determines the synchronization of the system, a city in our case, by measuring the time $\tau_{\text{sync}}(k)$ required to reach the synchronized state. The more heterogeneously distributed the initial phases are, the higher the time the system requires to synchronize. To distinguish between the effect produced by the spatial distribution x_i^k from its overall distribution as well as the topology of the graph, we also measure the average time the system needs to synchronize when the same phases are redistributed at random, $\tau_{\text{sync}}^{\text{null}}(k)$. The normalized synchronization time of the system is then given by the ratio

$$\tilde{\tau}_{\text{sync}}(k) = \frac{\tau_{\text{sync}}(k)}{\tau_{\text{sync}}^{\text{null}}(k)}. \tag{10}$$

Like for diffusion, a synchronization time close to one means that the spatial distribution of phases is compatible with the null model, and a larger value indicates that spatial heterogeneities delay the appearance of a synchronized state.

In **Figure 3A** we inspect the normalized synchronization time in Boston, Cleveland, Detroit and Denver when spatial units interact through Kuramoto-like dynamics. All four of them share similar features, with central classes displaying smaller synchronization times compared to the most disadvantaged and wealthier ones. An expected result since those individuals in the extremes of the income distribution tend to be more isolated and clustered together compared to middle-income citizens. Despite sharing qualitative features, the cities shown display sharp quantitative differences. Almost all categories

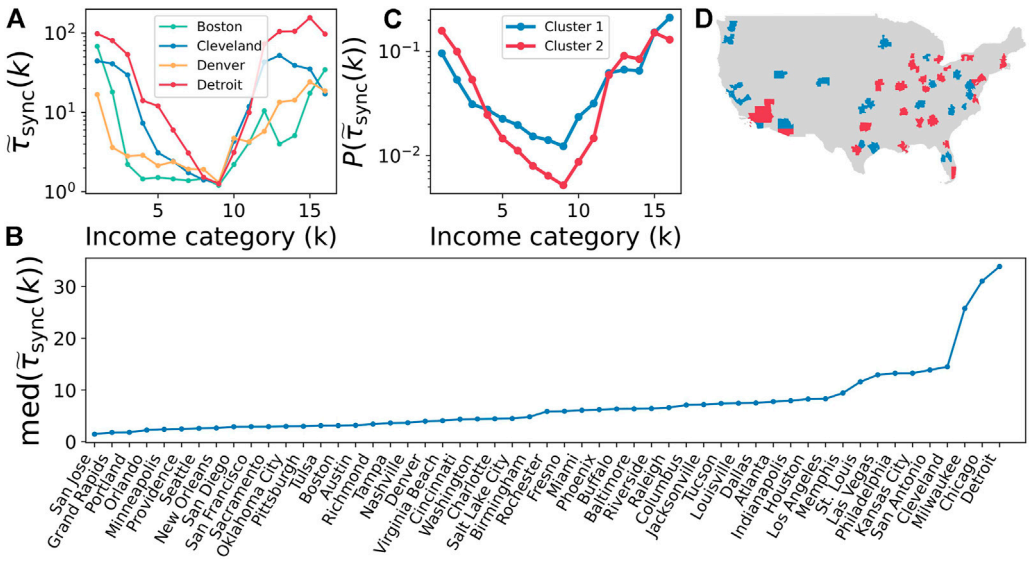

FIGURE 3 | Synchronization time as a measure for income segregation. **(A)** Synchronization time for each of the 16 income categories in Boston, Cleveland, Denver and Detroit. **(B)** Ranking for the median value of $\tilde{\tau}_{\text{sync}}(k)$ for the studied set of US cities. **(C)** Average value of $P(\tilde{\tau}_{\text{sync}}(k))$ as a function of each income category i for the two main clusters detected. **(D)** Location and cluster assignment for each of the analyzed cities.

appear to be significantly more isolated in Detroit and Cleveland compared to Denver and Boston, where $\tilde{\tau}_{\text{sync}}(k)$ looks much flat. Overall, the synchronization results are compatible with the diffusion ones, likely because both dynamical processes share common features. We have further checked that the mean x^k does not determine directly the normalized synchronization times in **Supplementary Figure S1**.

Likewise with diffusion, we calculate the median and variance of $\tilde{\tau}_{\text{sync}}(k)$ over all categories to be able to compare between analyzed cities (see **Supplementary Figure S2** for the individual rankings of $\tilde{\tau}_{\text{sync}}(k)$ for the categories $k = 1$ and $k = 16$). The ranking is shown in **Figure 3B** and has cities such as Detroit, Cleveland, Milwaukee or Memphis close to the top, which are well-known for being among the most economically segregated cities in the United States. The location in the ranking of the cities in **Figure 3A** is consistent with our observations, with Boston and Denver on the bottom of the ranking and Detroit and Cleveland on the top of it.

Our index is given by the median value of the normalized synchronization times, yet depending on the dimension of segregation we aim to capture, we can also construct an index based on a population-weighted average. Whereas the median gives equal weight to each economic category focusing on the segregation suffered by residents of category k, the weighted average provides an overall picture of segregation taking the population of each category into account. We show the ranking obtained for the weighted average index and its relation with $\text{med}(\tilde{\tau}_{\text{sync}}(k))$ in **Supplementary Figures S6, S7**. Additionally, we show in **Supplementary Figures S3, S4** how $\tilde{\tau}_{\text{sync}}(k)$ significantly correlates with the traditional Moran's I [54] as well as a multi-scale quantity based on class mean first passage times developed in [20, 21], reinforcing the idea that synchronization (and diffusion) dynamics indeed capture the patterns of residential segregation. Despite the dynamics we have used are stylized versions of the real behavior of the quantity x_i^k and do not capture the full complexity of its temporal evolution, it is able to capture segregation with values comparable to other segregation indicators.

Although $\tilde{\tau}_{\text{sync}}(k)$ is larger for extreme categories in most of the cities, some of them like Denver display smaller variations than others such as Detroit and, therefore, it might be of interest to group cities according to the change in synchronization times. By running a k-means algorithm on the normalized value of $P(\tilde{\tau}_{\text{sync}}(k))$ so that $\sum_k P(\tilde{\tau}_{\text{sync}}(k)) = 1$, we can split the cities of study between those with higher and smaller differences in $\tilde{\tau}_{\text{sync}}(k)$, see **Figure 3C**. In **Figure 3D**, we display the cluster assigned to each metropolitan area, where no strong spatial pattern is observed. Still, the cities in the Midwest, which are known for being economically segregated, fall into the red cluster, together with other cities such as Baltimore or Los Angeles. If, instead, we focus on the blue cluster, we have cities such as Sacramento or Washington D.C. Among the cities discussed in **Figure 3A**, Denver falls into the group with more homogeneous segregation (in blue) and the rest into the one with more unequal segregation patterns (in red).

Beyond the global quantification of segregation, we can also evaluate the local level of segregation of a concrete census tract i at a given time step t by computing

$$\rho_i^k(t) = \cos\left(\theta_i^k(t) - \Phi^k(t)\right), \tag{11}$$

where $\theta_i^k(t)$ is the phase of unit i at time t and $\Phi^k(t)$ is the average phase of all the oscillators in a city in a given time t [32]. When $\rho_i^k(t) > 0.999$ we consider that oscillator i has synchronized, from which we can obtain $\tau_i^{\text{loc}}(k)$. However, given that $\rho_i(\tau_i^{\text{loc}}(k))$ can oscillate through time, we only consider that a unit i has reached

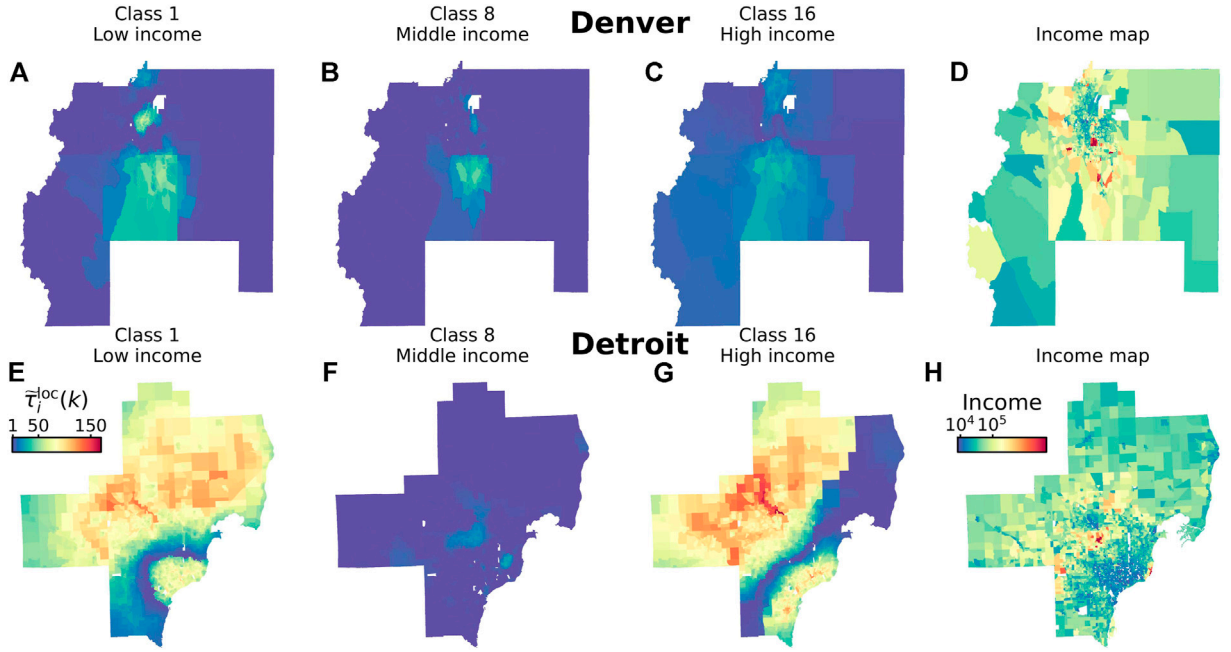

FIGURE 4 | Local synchronization time as a measure for income segregation. Normalized synchronization time for each census tract in Denver **(A–C)** and Detroit **(E–G)** for three different income categories: **(A,E)** class 1 (low income); **(B,F)** class 8 (middle income); **(C,G)** class 16 (high income). We provide as a reference the median income of each census tract in **(D)** Denver and **(H)** Detroit.

the global synchronized state at a time $\tau_i^{\mathrm{loc}}(k)$ when $\rho_i(t > \tau_i^{\mathrm{loc}}(k))$ does not go below 0.999 anymore, otherwise our methodology could fail to capture long-range correlations. In order to provide a metric for each spatial unit, simulations last until each of the spatial units have fullfiled the synchronization criteria. Normalizing $\tau_i^{\mathrm{loc}}(k)$ by its null model counterpart, it yields $\tilde{\tau}_i^{\mathrm{loc}}(k)$, a measure of the local synchronization time.

Figure 4 displays the normalized synchronization times for each of the census tracts in Denver and Detroit, focusing on three very distinct income categories: low income, **Figures 4A,E**; middle income, **Figures 4B,F**; and high income, **Figures 4C,G**. To ease the comparison between income categories, the range of values is common for all the maps, evincing the strong differences between Detroit and Denver, especially for the low and high-income categories. **Figures 4D,H** also report the income per census tract. The shape of the segregation in Detroit can be outlined by the lower-income downtown and the richer suburbs, being the most segregated parts, and a less-segregated region in-between. In the case of Denver, we only slightly see high values for the low-income category in the North of the city and the high-income category in the South.

As we detail in **Supplementary Figure S5**, the spatial patterns of segregation product of the synchronization dynamics are significantly different to those obtained from first-neighbor quantities such as the Moran's I. Instead of focusing on those regions whose proportion of citizens is high (or low) compared to its neighbors, our methodology highlights those with a ratio of population within a category k distinct than the average, either because it is high or low, and spatially isolated from those regions with average values. In other words, a region with a high proportion of residents of category k might not show a large local spatial correlation if their neighbors have similar values but could, instead, produce high values of $\tilde{\tau}_i^{\mathrm{loc}}(k)$ if it is isolated from those regions displaying a proportion of citizens closer to the city average. As the majority of spatial measures, our approach can also suffer the so-called modifiable areal unit problem [55] in a similar fashion. However, given that our methodology captures mid and long-range correlations instead of local differences, it might be less affected by such small local changes.

Finally, we inspect if the synchronization time of a region displays any type of connection with its actual income. To do so, we plot in **Figure 5** the normalized local synchronization time as a function of the median income averaged over all the census tracts within bins of $5,000 in four US cities. Again we see that segregation is much stronger in Detroit followed by Cleveland and Boston. High-income regions are more segregated in Boston compared to Cleveland. In general terms, the census tracts with a median income between $50,000 and $80,000 seem to be the less segregated ones as they synchronize faster for both low and high-income categories. These results are in agreement with the cluster assignment of the previous cities, with Detroit, Cleveland and Boston in the red cluster where low and high-income categories need more time to synchronize, and Denver in the blue cluster where only the high-income categories need more time to synchronize.

3 DISCUSSION

Traditional spatial segregation indicators that focus on local scale of segregation fail in most cases to capture the presence of

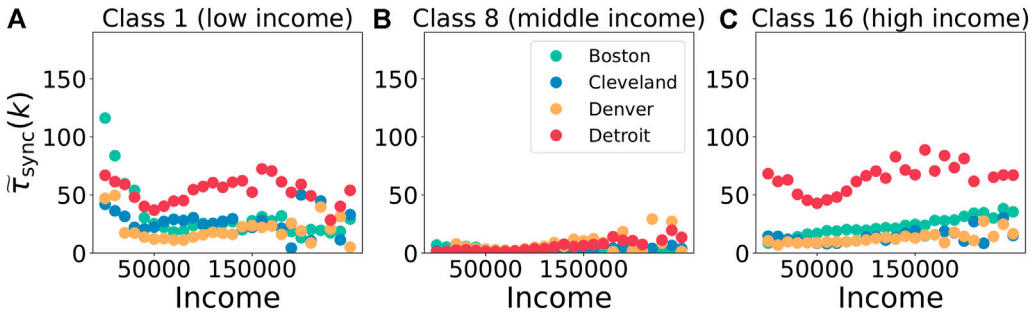

FIGURE 5 | Synchronization time and median income. Normalized synchronization time as a function of the median income averaged over bins of $5,000 for class 1 **(A)**, class 8 **(B)** and class 16 **(C)**.

long-range correlations, thus highlighting the need of multi-scale indices [15–21]. Our framework does not consider any specific scale, but uses a dynamical approach that captures the patterns of segregation across the multiple scales. We have revealed how categories in the extreme of the income distribution are more heterogeneously distributed in space compared to middle classes, displaying larger diffusion and synchronization times. This approach has also allowed us to group together those cities that display common features of segregation. In this context, it is important to note that our work does not attempt to model the evolution of income segregation nor can be used as a forecasting tool, but takes modeling assumptions to assess the level of segregation that a distribution of population exhibits.

Despite the main manuscript focuses on the economic segregation, our methodology can be used to assess the heterogeneity in the spatial distribution of any characteristic. Moreover, it can go beyond the spatial component of segregation by including in the analysis other types of graphs, e.g., the daily mobility network of citizens. In this way, we could assess how citizens of diverse socioeconomic environments interact through mobility [56–59].

Summarizing, we show how diffusion and synchronization dynamics can be used in some systems to assess the heterogeneity in the distribution of node features. While the present work focuses on the initial phases of oscillators and their synchronization time, node metadata could also be understood as an internal frequency and provide further insights on feature correlation across topological scales.

DATA AVAILABILITY STATEMENT

Publicly available datasets were analyzed in this study. This data can be found here: https://www.census.gov/programs-surveys/acs.

AUTHOR CONTRIBUTIONS

AB performed the research. AB, SG, and AA designed the research and wrote the manuscript.

FUNDING

AB acknowledges financial support from the Ministerio de Ciencia e Innovación under the Juan de la Cierva program (FJC2019-038958-I). We acknowledge support by Ministerio de Economía y Competitividad (PGC2018-094754-BC21, FIS2017-90782-REDT and RED2018-102518-T), Generalitat de Catalunya (2017SGR-896 and 2020PANDE00098), and Universitat Rovira i Virgili (2019PFR-URV-B2-41). AA acknowledges also ICREA Academia and the James S. McDonnell Foundation (220020325).

SUPPLEMENTARY MATERIAL

The Supplementary Material for this article can be found online at: https://www.frontiersin.org/articles/10.3389/fphy.2022.833426/full#supplementary-material

REFERENCES

1. Kennedy BP, Kawachi I, Glass R, Prothrow-Stith D. Income Distribution, Socioeconomic Status, and Self Rated Health in the united states: Multilevel Analysis. *BMJ* (1998) 317:917–21. doi:10.1136/bmj.317.7163.917
2. Elliott JR. Social Isolation and Labor Market Insulation: Network and Neighborhood Effects on Less-Educated Urban Workers. *Sociological Q* (1999) 40:199–216. doi:10.1111/j.1533-8525.1999.tb00545.x
3. Collins WJ, Margo RA. Residential Segregation and Socioeconomic Outcomes. *Econ Lett* (2000) 69:239–43. doi:10.1016/s0165-1765(00)00300-1
4. Ross NA, Nobrega K, Dunn J. Income Segregation, Income Inequality and Mortality in north American Metropolitan Areas. *GeoJournal* (2001) 53: 117–24. doi:10.1023/a:1015720518936
5. Mayer SE. How Economic Segregation Affects Children's Educational Attainment. *Social Forces* (2002) 81:153–76. doi:10.1353/sof.2002.0053
6. Acevedo-Garcia D, Lochner KA. *Residential Segregation and Health*. Neighborhoods and Health (2003). p. 265–87. doi:10.1093/acprof:oso/9780195138382.003.0012Residential Segregation and Health
7. Wheeler CH. *Urban Decentralization and Income Inequality: Is Sprawl Associated with Rising Income Segregation across Neighborhoods?* FRB of St. Louis (2006). Working Paper No. 2006–037A.

8. Owens A. Income Segregation between School Districts and Inequality in Students' Achievement. *Sociol Educ* (2018) 91:1–27. doi:10.1177/0038040717741180
9. Cliff AD, Ord JK. *Spatial Processes: Models & Applications*. Taylor & Francis (1981).
10. Dawkins CJ. Measuring the Spatial Pattern of Residential Segregation. *Urban Stud* (2004) 41:833–51. doi:10.1080/0042098042000194133
11. Brown LA, Chung S-Y. Spatial Segregation, Segregation Indices and the Geographical Perspective. *Popul Space Place* (2006) 12:125–43. doi:10.1002/psp.403
12. Dawkins C. The Spatial Pattern of Black-white Segregation in Us Metropolitan Areas: an Exploratory Analysis. *Urban Stud* (2006) 43:1943–69. doi:10.1080/00420980600897792
13. Wong DWS, Shaw S-L. Measuring Segregation: An Activity Space Approach. *J Geogr Syst* (2011) 13:127–45. doi:10.1007/s10109-010-0112-x
14. Rey SJ, Smith RJ. A Spatial Decomposition of the Gini Coefficient. *Lett Spat Resour Sci* (2013) 6:55–70. doi:10.1007/s12076-012-0086-z
15. Farber S, Páez A, Morency C. Activity Spaces and the Measurement of Clustering and Exposure: A Case Study of Linguistic Groups in Montreal. *Environ Plan A* (2012) 44:315–32. doi:10.1068/a44203
16. Louf R, Barthelemy M. Patterns of Residential Segregation. *PLOS ONE* (2016) 11:e0157476. doi:10.1371/journal.pone.0157476
17. Chodrow PS. Structure and Information in Spatial Segregation. *Proc Natl Acad Sci U.S.A* (2017) 114:11591–6. doi:10.1073/pnas.1708201114
18. Olteanu M, Randon-Furling J, Clark WAV. Segregation through the Multiscalar Lens. *Proc Natl Acad Sci U.S.A* (2019) 116:12250–4. doi:10.1073/pnas.1900192116
19. Sousa S, Nicosia V. *Quantifying Ethnic Segregation in Cities through Random Walks* (2020). *arXiv* (2020) arXiv:2010.10462.
20. Bassolas A, Nicosia V. First-passage Times to Quantify and Compare Structural Correlations and Heterogeneity in Complex Systems. *Commun Phys* (2021) 4:1–14. doi:10.1038/s42005-021-00580-w
21. Bassolas A, Sousa S, Nicosia V. Diffusion Segregation and the Disproportionate Incidence of Covid-19 in African American Communities. *J R Soc Interf* (2021) 18:20200961. doi:10.1098/rsif.2020.0961
22. Gómez S, Díaz-Guilera A, Gómez-Gardeñes J, Pérez-Vicente CJ, Moreno Y, Arenas A. Diffusion Dynamics on Multiplex Networks. *Phys Rev Lett* (2013) 110:028701. doi:10.1103/PhysRevLett.110.028701
23. Solé-Ribalta A, De Domenico M, Kouvaris NE, Díaz-Guilera A, Gómez S, Arenas A. Spectral Properties of the Laplacian of Multiplex Networks. *Phys Rev E Stat Nonlin Soft Matter Phys* (2013) 88:032807. doi:10.1103/PhysRevE.88.032807
24. De Domenico M, Solé-Ribalta A, Cozzo E, Kivelä M, Moreno Y, Porter MA, et al. Mathematical Formulation of Multilayer Networks. *Phys Rev X* (2013) 3:041022. doi:10.1103/physrevx.3.041022
25. Li Y, Chen W, Wang Y, Zhang ZL. Influence Diffusion Dynamics and Influence Maximization in Social Networks with Friend and Foe Relationships. *Proc sixth ACM Int Conf Web search Data mining* (2013) 657–66. doi:10.1145/2433396.2433478
26. Delvenne JC, Lambiotte R, Rocha LE. Diffusion on Networked Systems Is a Question of Time or Structure. *Nat Commun* (2015) 6:7366–10. doi:10.1038/ncomms8366
27. De Domenico M. Diffusion Geometry Unravels the Emergence of Functional Clusters in Collective Phenomena. *Phys Rev Lett* (2017) 118:168301. doi:10.1103/physrevlett.118.168301
28. Masuda N, Porter MA, Lambiotte R. Random Walks and Diffusion on Networks. *Phys Rep* (2017) 716-717:1–58. doi:10.1016/j.physrep.2017.07.007
29. Cencetti G, Battiston F. Diffusive Behavior of Multiplex Networks. *New J Phys* (2019) 21:035006. doi:10.1088/1367-2630/ab060c
30. Bertagnolli G, De Domenico M. Diffusion Geometry of Multiplex and Interdependent Systems. *Phys Rev E* (2021) 103:042301. doi:10.1103/PhysRevE.103.042301
31. Arenas A, Díaz-Guilera A, Pérez-Vicente CJ. Synchronization Processes in Complex Networks. *Physica D: Nonlinear Phenomena* (2006) 224:27–34. doi:10.1016/j.physd.2006.09.029
32. Arenas A, Díaz-Guilera A, Pérez-Vicente CJ. Synchronization Reveals Topological Scales in Complex Networks. *Phys Rev Lett* (2006) 96:114102. doi:10.1103/physrevlett.96.114102
33. Gómez-Gardeñes J, Moreno Y, Arenas A. Paths to Synchronization on Complex Networks. *Phys Rev Lett* (2007) 98:034101. doi:10.1103/PhysRevLett.98.034101
34. Gómez-Gardeñes J, Moreno Y, Arenas A. Synchronizability Determined by Coupling Strengths and Topology on Complex Networks. *Phys Rev E Stat Nonlin Soft Matter Phys* (2007) 75:066106. doi:10.1103/PhysRevE.75.066106
35. Arenas A, Díaz-Guilera A, Kurths J, Moreno Y, Zhou C. Synchronization in Complex Networks. *Phys Rep* (2008) 469:93–153. doi:10.1016/j.physrep.2008.09.002
36. Gómez-Gardeñes J, Soriano-Paños D, Arenas A. Critical Regimes Driven by Recurrent Mobility Patterns of Reaction-Diffusion Processes in Networks. *Nat Phys* (2018) 14:391–5. doi:10.1038/s41567-017-0022-7
37. Zhang Z-K, Liu C, Zhan X-X, Lu X, Zhang C-X, Zhang Y-C. Dynamics of Information Diffusion and its Applications on Complex Networks. *Phys Rep* (2016) 651:1–34. doi:10.1016/j.physrep.2016.07.002
38. Pluchino A, Latora V, Rapisarda A. Changing Opinions in a Changing World: A New Perspective in Sociophysics. *Int J Mod Phys C* (2005) 16:515–31. doi:10.1142/s0129183105007261
39. Calderón C, Chong A, Stein E. Trade Intensity and Business Cycle Synchronization: Are Developing Countries Any Different? *J Int Econ* (2007) 71:2–21. doi:10.1016/j.jinteco.2006.06.001
40. Erola P, Díaz-Guilera A, Gómez S, Arenas A. *Modeling International Crisis Synchronization in the World Trade Web*, 7. Networks and Heterogeneous Media (2012). 385–97. doi:10.3934/nhm.2012.7.385Modeling International Crisis Synchronization in the World Trade Web*Nhm*
41. Motter AE, Zhou C, Kurths J. Network Synchronization, Diffusion, and the Paradox of Heterogeneity. *Phys Rev E Stat Nonlin Soft Matter Phys* (2005) 71:016116. doi:10.1103/PhysRevE.71.016116
42. Schelling TC. Dynamic Models of Segregation†. *J Math Sociol* (1971) 1:143–86. doi:10.1080/0022250x.1971.9989794
43. Fujita M. *Urban Economic Theory*. Cambridge University Press (1989).
44. Zhang J. A Dynamic Model of Residential Segregation. *J Math Sociol* (2004) 28:147–70. doi:10.1080/00222500490480202
45. Clark WAV. Changing Residential Preferences across Income, Education, and Age. *Urban Aff Rev* (2009) 44:334–55. doi:10.1177/1078087408321497
46. Zhang J. Tipping and Residential Segregation: a Unified Schelling Model*. *J Reg Sci* (2011) 51:167–93. doi:10.1111/j.1467-9787.2010.00671.x
47. DeLuca S, Garboden PME, Rosenblatt P. Segregating Shelter. *Annals Am Acad Polit Soc Sci* (2013) 647:268–99. doi:10.1177/0002716213479310
49. Adelman RM. Neighborhood Opportunities, Race, and Class: The Black Middle Class and Residential Segregation. *City & Community* (2004) 3:43–63. doi:10.1111/j.1535-6841.2004.00066.x
50. Thomas M, Moye R. Race, Class, and Gender and the Impact of Racial Segregation on Black-white Income Inequality. *Sociol Race Ethn* (2015) 1:490–502. doi:10.1177/2332649215581665
51. Florida R, Mellander C. *Segregated City: The Geography of Economic Segregation in America's Metros*. Martin Prosperity Institute (2015).
52. Hartigan JA, Wong MA. Algorithm as 136: A K-Means Clustering Algorithm. *Appl Stat* (1979) 28:100–8. doi:10.2307/2346830
53. Likas A, Vlassis N, J. Verbeek J. The Global K-Means Clustering Algorithm. *Pattern Recognition* (2003) 36:451–61. doi:10.1016/s0031-3203(02)00060-2
54. Moran PAP. The Interpretation of Statistical Maps. *J R Stat Soc Ser B (Methodological)* (1948) 10:243–51. doi:10.1111/j.2517-6161.1948.tb00012.x
55. Fotheringham AS, Wong DWS. The Modifiable Areal Unit Problem in Multivariate Statistical Analysis. *Environ Plan A* (1991) 23:1025–44. doi:10.1068/a231025
56. Xu Y, Belyi A, Santi P, Ratti C. Quantifying Segregation in an Integrated Urban Physical-Social Space. *J R Soc Interf* (2019) 16:20190536. doi:10.1098/rsif.2019.0536
57. Tóth G, Wachs J, Di Clemente R, Á J, Ságvári B, Kertész J, et al. Inequality Is Rising where Social Network Segregation Interacts with Urban Topology. *Nat Commun* (2021) 12:1–9. doi:10.1038/s41467-021-21465-0

58. Bokányi E, Juhász S, Karsai M, Lengyel B. Universal Patterns of Long-Distance Commuting and Social Assortativity in Cities. *Scientific Rep* (2021) 11:1–10. doi:10.1038/s41598-021-00416-1
59. Moro E, Calacci D, Dong X, Pentland A. Mobility Patterns Are Associated with Experienced Income Segregation in Large Us Cities. *Nat Commun* (2021) 12: 4633–10. doi:10.1038/s41467-021-24899-8
60. Manson S, Schroeder J, Riper DV, Ruggles S. *IPUMS National Historical Geographic Information System: Version 14.0 [Database]*. Minneapolis, MN: IPUMS (2019). [Dataset]. doi:10.18128/D050.V14.0

Conflict of Interest: The authors declare that the research was conducted in the absence of any commercial or financial relationships that could be construed as a potential conflict of interest.

Publisher's Note: All claims expressed in this article are solely those of the authors and do not necessarily represent those of their affiliated organizations, or those of the publisher, the editors and the reviewers. Any product that may be evaluated in this article, or claim that may be made by its manufacturer, is not guaranteed or endorsed by the publisher.

frontiers

Supplementary Material for "Diffusion and synchronization dynamics reveal the multi-scale patterns of spatial segregation"

Aleix Bassolas *, **Sergio Gómez and Alex Arenas**

Departament d'Enginyeria Informàtica i Matemàtiques, Universitat Rovira i Virgili, Tarragona, Spain

*Correspondence: aleix.bassolas@urv.cat

1 SUPPLEMENTARY RESULTS FOR DIFFUSION AND SYNCHRONIZATION DYNAMICS AND ECONOMIC SEGREGATION

We provide here supplementary results related to the study of income segregation in US cities. Figure S1 reports (A) the mean and (B) standard deviation of x_i^k in Boston, Cleveland, Detroit and Denver. Both of them reach minimum values between 8-10.

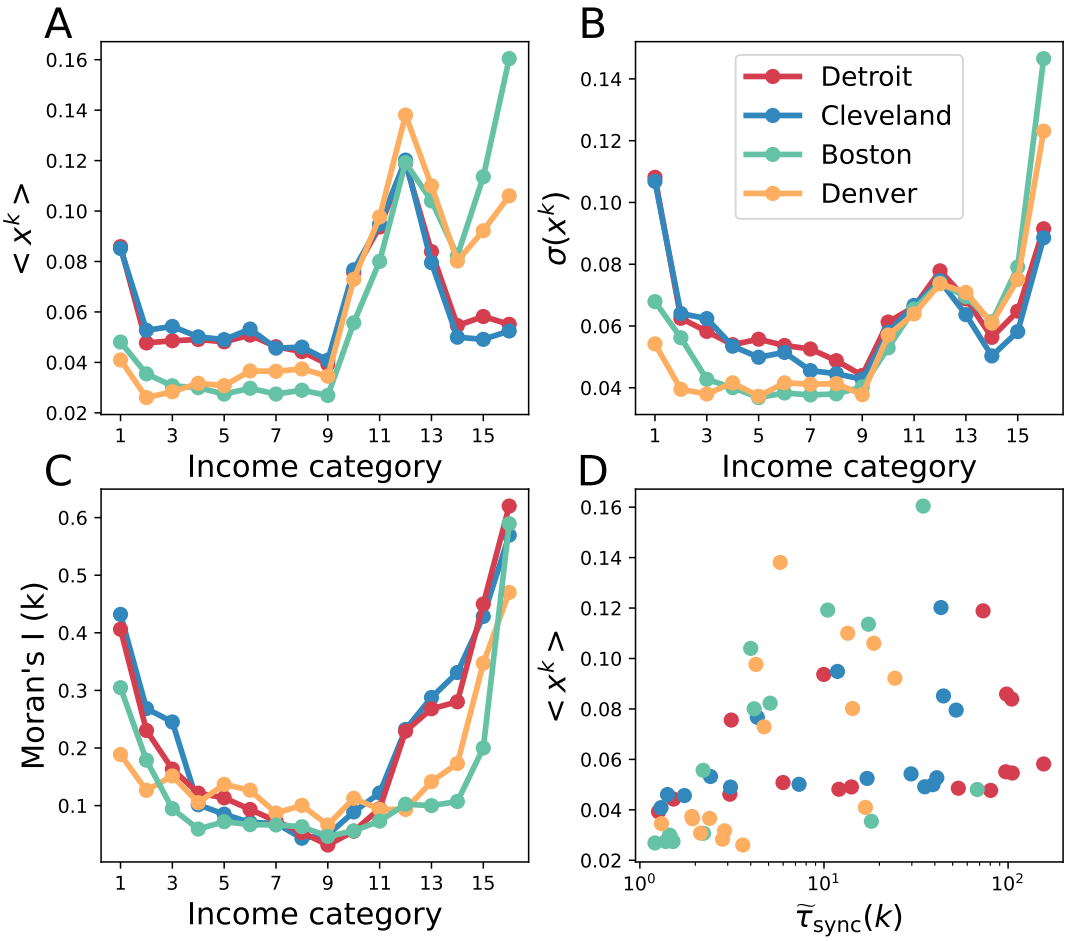

Figure S1. (A) Mean of x^k for each income category in Boston, Cleveland, Detroit and Denver. (B) Standard deviation $\sigma(x^k)$ for each income category in Boston, Cleveland, Detroit and Denver. (C) Moran's I for each income category in Boston, Cleveland, Detroit and Denver. (D) Scatter plot of the mean of x^k as a function of $\widetilde{\tau}_{\text{sync}}(k)$.

The fact that classes 8-10 appear to be the less segregated is also supported by the Moran's I as Fig. S1(C) shows. To further assess that the mean $< x^k >$ does not strongly determine the values of $\widetilde{\tau}_{\rm sync}(k)$, we plot both quantities in Fig. S1(D), where no strong pattern is observed. Categories with low $< x^k >$ display high variability in $\widetilde{\tau}_{\rm sync}(k)$ and vice-versa.

In Fig. S2 we provide the ranking of the selected US cities according to the value of $\widetilde{\tau}_{\rm sync}(k)$ for the lowest and highest income categories 1 and 16, respectively. As can be seen, there are significant variations in the ranking depending on which economic category is shown; for example, Cleveland is close to the top for category 1 but far apart for 16, and the other way around for Seattle.

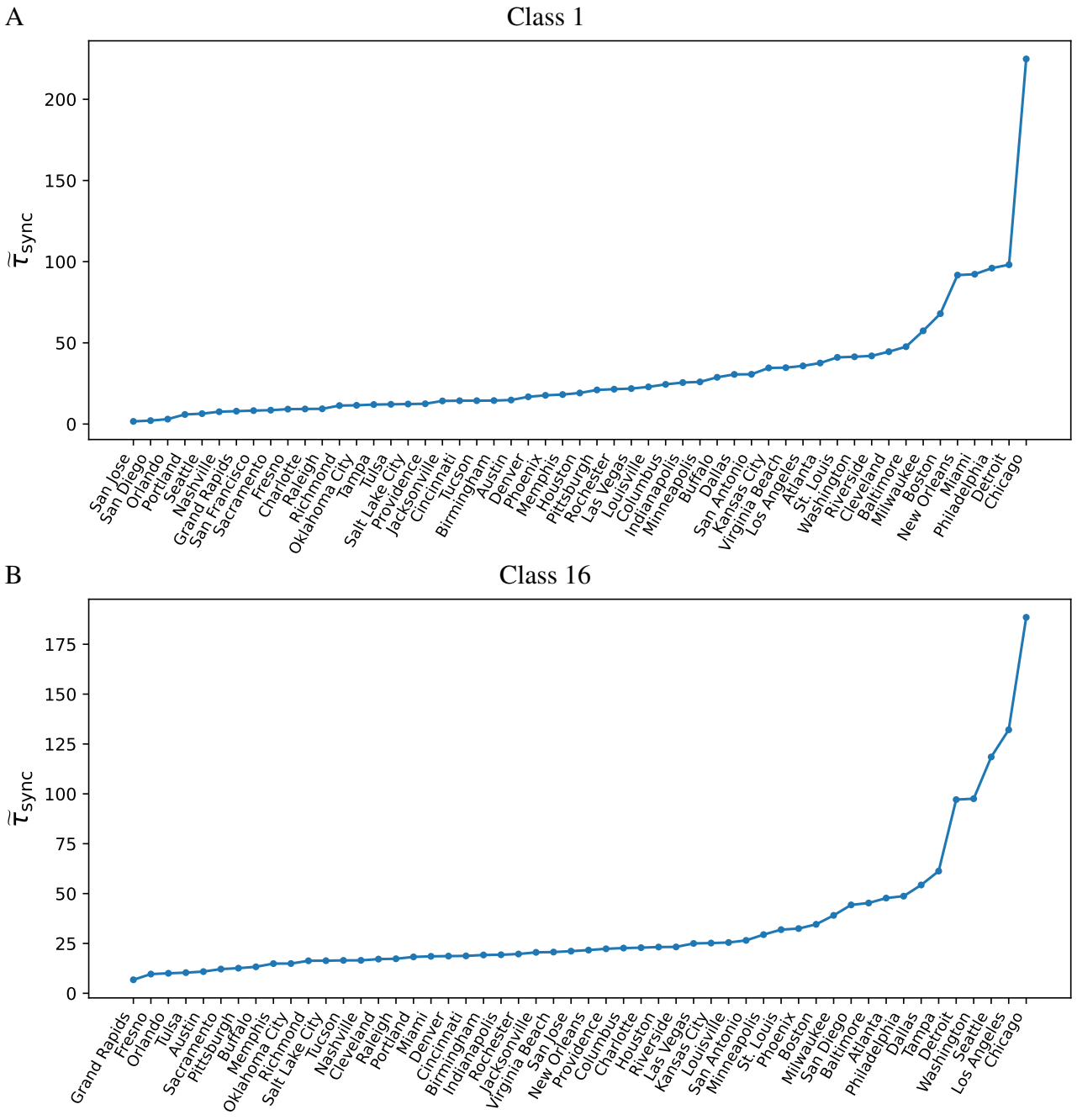

Figure S2. Ranking of the selected US cities according to the value of $\widetilde{\tau}_{\rm sync}(k)$, for income class 1 (A) and income class 16 (B).

2 COMPARISON WITH OTHER SEGREGATION MEASURES

In this section we assess how the normalized synchronization time $\widetilde{\tau}^k_{\rm sync}$ relates to other segregation measures. In particular we focus on the widely used Moran's I [1], which focuses on local correlations, and one obtained from class mean first passage times (CMFPT) developed in [2, 3], which captures long-range spatial correlations.

For each city and category k the Moran's I can be written as

$$I^k = \frac{\frac{1}{W}\sum_{i=1}^{n}\sum_{j=1}^{n} w_{ij}(x_i^k - \bar{x}^k)(x_j^k - \bar{x}^k)}{\frac{1}{n}\sum_{i=1}^{n}(x_i^k - \bar{x}^k)^2}, \tag{S1}$$

where x_i^k is the fraction of population in i that belongs to category k, $\bar{x}^k$ is its mean across all spatial units, the weights w_{ij} correspond in our case to the spatial adjacency matrix a_{ij}, and $W = \sum_{i=1}^{n}\sum_{j=1}^{n} w_{ij}$ is the total weight.

As an index to assess the long-range correlations in the spatial distribution of the income categories, we will use the class mean first passage times between classes. In this methodology [2, 3], random walkers start from each of the spatial units in a system and move through the spatial adjacency graph until they have visited the 16 classes at least once. For this, each location is assigned to a class with probability proportional to its corresponding fraction of population. By averaging the number of steps that a walker needs to reach class j across all the units that belong to category i and for multiple realizations, we can obtain the class mean first passage times τ_{ij}, which encapsulate the average number of steps needed to reach a unit of category j when a walker departs from a unit of category i. After normalizing by a null-model in which colors are uniformly reshuffled at random to compensate for uneven class abundances, we finally obtain the normalized class mean first passage times $\widetilde{\tau}_{ij}$. The quantity $\widetilde{\tau}_{ij}$ provides thus information on how much time you need to reach category j when a walker departs from a unit of category i as compared to the null-model, values below 1 mean that two categories are closer than in the null-model and vice-versa for values above 1. To summarize the segregation of category k in a city we will use the CMFPT index, i.e., the $\text{med}(\widetilde{\tau})_k$ given by the median value of τ_{jk} $\forall j$.

For each city included in our analysis, we measure the Pearson correlation coefficient r_p between each of the additional segregation quantities and $\widetilde{\tau}^k_{\rm sync}$ for all the 16 categories k. More specifically, for each city r_p is calculated over a set of 16 points. The distribution of r_p across cities is shown in Fig. S3 for the Moran's I (A) and $\text{med}(\widetilde{\tau})_k$ (B), where a skewness towards high values is clearly observed. Most of the cities display correlations above 0.8 with the Moran's I and 0.7 with the CMFPT index. Additionally, we also show in Fig. S4 the significance of the correlations observed in each of the cities, which are also below 0.001 in most of the cases.

In the main text we discuss the potential of our methodology to assess the multiscale patterns of segregation in front of traditional first-neighbor approaches. In Fig. S5 we further investigate this fact by plotting for Boston, Cleveland, Denver and Detroit the local normalized synchronization times, the local Moran's $I_i^{\mathrm{loc}}(k)$, and the raw ratio of population of category k in each of the census tracts.

Although the segregation hotspots detected by our methodology and the local Moran's I seem similar, the patterns detected are significantly different. Whereas $I_i^{\mathrm{loc}}(k)$ captures strong differences between

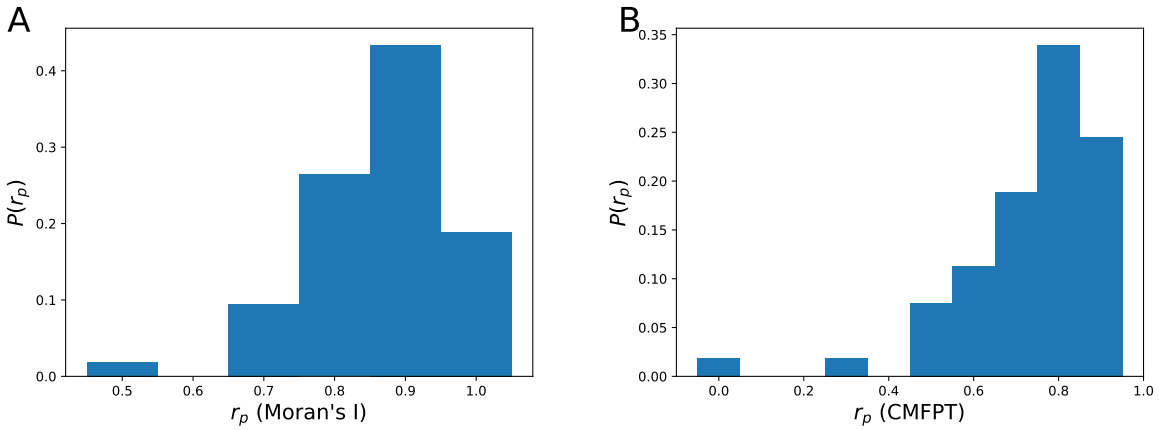

Figure S3. Correlation between $\widetilde{\tau}^k_{\mathrm{sync}}$ and the additional segregation indicators. For each city in our study, we calculate the Pearson correlation coefficient r_p between $\widetilde{\tau}^k_{\mathrm{sync}}$ and the additional segregation metrics over the 16 income categories. The correlation coefficient for a city is thus obtained from a set of 16 points, one per category. (A) Distribution of r_p between Moran's I and $\widetilde{\tau}^k_{\mathrm{sync}}$ across cities. (B) Distribution of r_p between the segregation calculated through normalized CMFPT $\mathrm{med}(\widetilde{\tau})_k$ and $\widetilde{\tau}^k_{\mathrm{sync}}$ across cities.

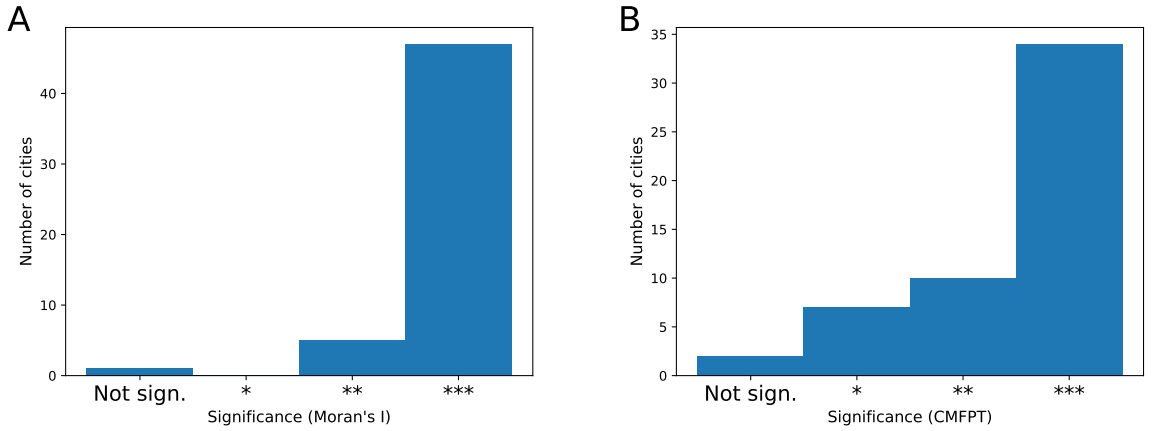

Figure S4. Significance of the Pearson correlation coefficients between $\widetilde{\tau}^k_{\mathrm{sync}}$ and the other segregation indicators. For each of the additional indices, we display the significance of the correlations across cities. (A) Significance of correlations between Moran's I and $\widetilde{\tau}^k_{\mathrm{sync}}$. (B) Significance of correlations between the segregation calculated through normalized class mean first passage times $\mathrm{med}(\widetilde{\tau})_i$ and $\widetilde{\tau}^k_{\mathrm{sync}}$. The correlation coefficient and significance for each city is obtained by comparing the segregation values for the 16 income categories. The significance values are depicted as * for p-value < 0.05, ** for p-value < 0.01, and *** for p-value < 0.001.

neighboors, $\widetilde{\tau}_i^{\mathrm{loc}}(k)$ highlights isolated regions even if the differences with their first-neighboors is low; most likely, this is because they are far apart from regions displaying ratios of population closer to the city average and require more time to reach the global synchronized state. In fact, the areas highlighted by synchronization dynamics have a larger scale and allow us to identify common mesoscale patterns of segregation across cities: a downtown that displays high values, a ring around it with low values, and finally the suburbs with high values again. By focusing on Detroit, we can see that not only the poorer downtown appears highlighted but also the suburbs due to their very low ratio of population of category 1. Similar patterns can also be observed in Cleveland and Denver.

The segregation index developed in the main text is calculated as the median of $\widetilde{\tau}_{\mathrm{sync}}^k$ which confers an equal weight to each of the income categories, disregarding the amount of population in each category. However, we can also construct a weighted index $\widetilde{\widetilde{\tau}}_{\mathrm{sync}}$ that can be built as

$$\widetilde{\widetilde{\tau}}_{\mathrm{sync}} = \frac{\sum_k P_k \widetilde{\tau}_{\mathrm{sync}}(k)}{\sum_k P_k}, \tag{S2}$$

where P_k is the total number of citizens that belong to category k in a given city. The ranking of cities according to the value of $\widetilde{\widetilde{\tau}}_{\mathrm{sync}}$ (Fig. S6) displays only slight changes with, for example, Philadelphia and Los Angeles closer to the top of the ranking. We test the relation between both indices in Fig. S7, where a clear relationship between both quantities is revealed.

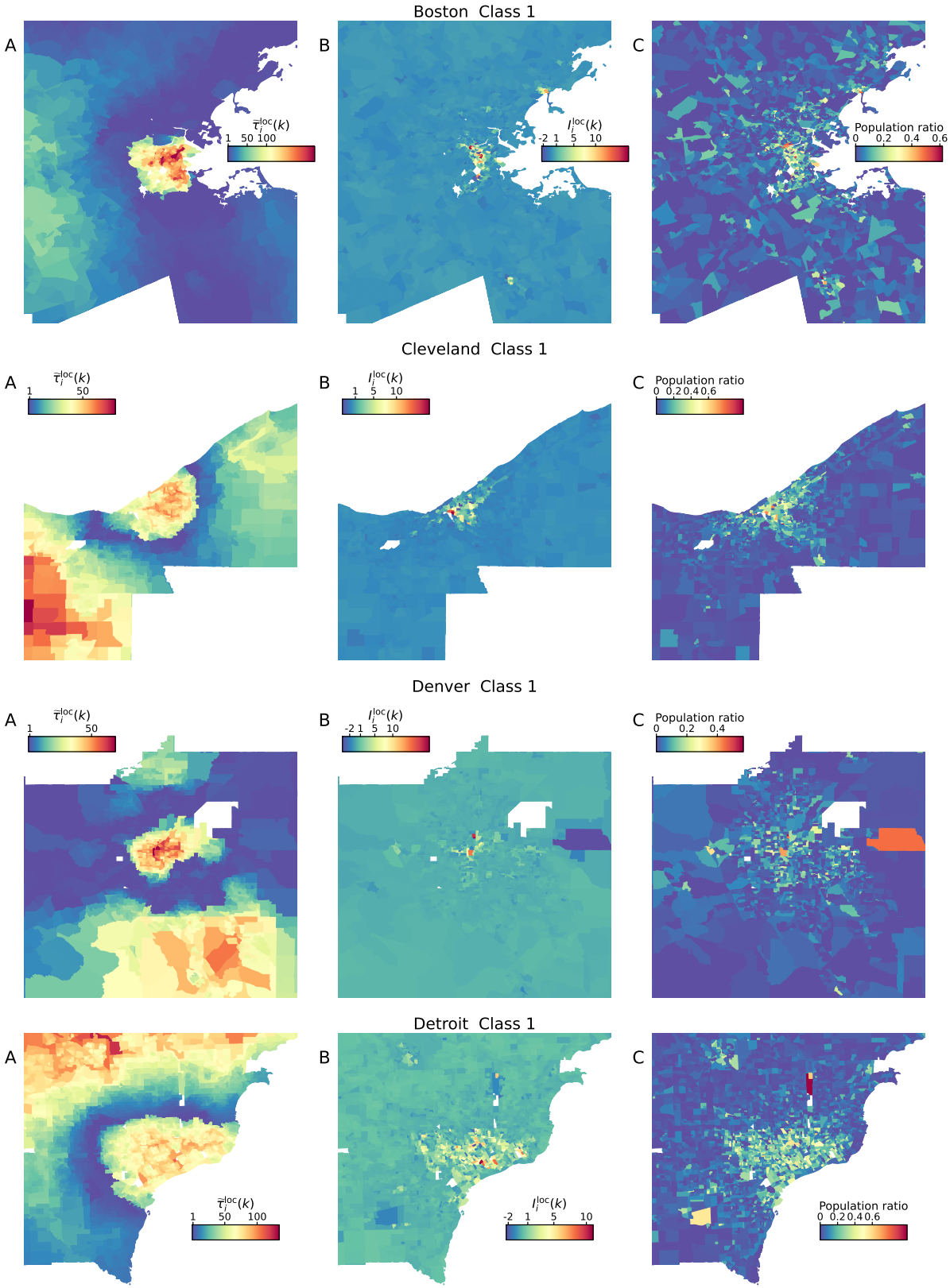

Figure S5. Comparison of local segregation indicators in Boston, Cleveland, Denver and Detroit. (A) Normalized synchronization time, (B) Local Moran correlation, and (C) proportion of citizens for each census tract and income class 1 (most deprived).

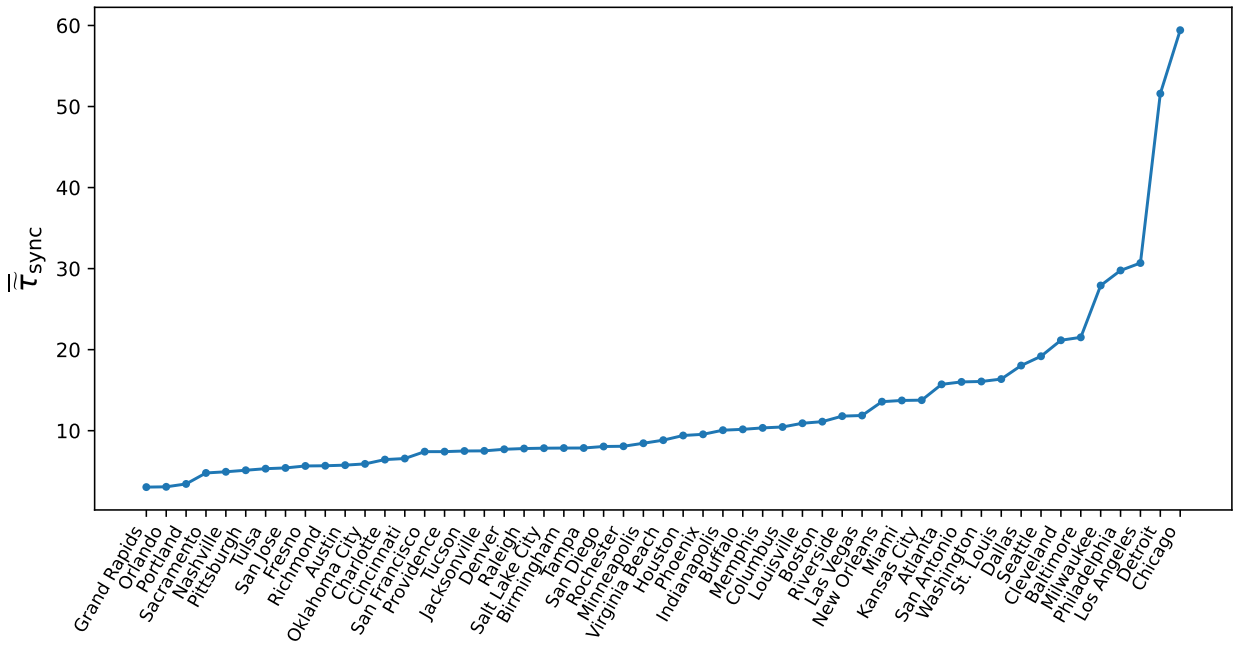

Figure S6. Segregation in US cities according to an index calculated through a weighted average. Ranking of cities according to the weighted index of segregation $\widetilde{\overline{\tau}}_{\text{sync}}$.

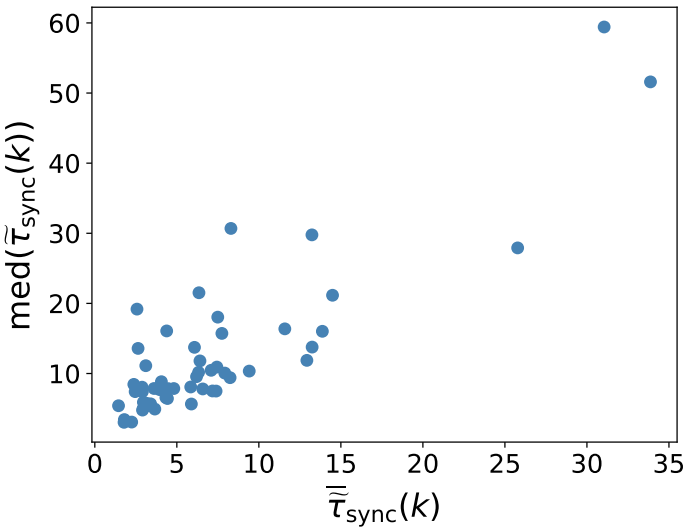

Figure S7. Comparison between segregation indicators obtained through synchronization dynamics. Comparison between the weighted index of segregation $\widetilde{\overline{\tau}}_{\text{sync}}$ and the index $\text{med}(\widetilde{\tau}_{\text{diff}}(k))$ used in the main text.

3 BEYOND ECONOMIC SEGREGATION: PARIS AROUND THE CLOCK

Besides only economic segregation, our methodology can be used to assess the spatial heterogeneity of any other quantity, and to exemplify it, we assess in this section the segregation of the population in Paris according to a wide set of socioeconomic indicators. The data compiles the fraction of population per district within a certain category at each hour of the day in French cities; in this work, we focus on Paris [4, 5, 6]. The list of indicators and categories analyzed can be found in Table S1.

Indicator	Categories				
Activity type	At home	At work	Studying	Shopping	Leisure
Age	16-24	25-34	35-64	65 and more	
Educational level	Low	Middle-low	Middle-high	High	
Socioprofessional status	Inactive	Low	Middle-low	Middle-high	High
Last travel mode	Pub. trans.	Private motor	Soft mobility		
Occupational status	Active	Student	Unemployed	Retired	Inactive
Sex	Male	Female			

Table S1. Socio-economic indicators and activity types analyzed for Paris.

For each indicator or category, we have a certain distribution of population per spatial unit and hour of the day, thus we can compute how the quantity $\widetilde{\tau}_{\rm sync}(k)$ varies during the day, as we show in Fig. S8(A,B) for the five activity types, and the five socio-professional status; the patterns of synchronization through time turn out to be very distinct. For example, the level of synchronization remains basically constant throughout the day for low, middle and high socio-professional status, while it increases (decreases) between 8am and 8pm for inactive (high) socio-professional status. If we focus instead on the ranking of $\widetilde{\tau}_{\rm sync}(k)$ at 10am and 10pm, see Fig. S8(C), the lower occupational and socio-professional status seem to be the most segregated indicators as they are on top of the ranking at both times of the day. Other categories that should be uniformly distributed across the city, such as sex, are very close to 1, thus indicating no segregation.

The hourly patterns of each metric allow for the grouping of indicators behaving similarly as we did for US cities. As before, we focus more on the time-series profile rather than the specific values taken by bon $\widetilde{\tau}^h_{\rm sync}(k)$, thus analyzing the normalized $P(\widetilde{\tau}^h_{\rm sync}(k))$ for each hour of the day h. The k-means clustering reveals four distinct clusters (see Fig. S9) which correspond to: those increasing during workings, those decreasing, those remaining almost constant, and those with a more characteristic behavior with a peak during midday and at the end of the day, roughly around the lunch and dinner times.

Finally, we assess the local segregation of districts by measuring their local normalized synchronization time. In particular, we show an example in Fig. S10 for the population performing leisure activities and those with inactive socio-professional status. In agreement with the temporal pattern shown in Fig. S8, the segregation is much higher at 10pm compared to 10am, especially concentrated in the centre of the city; a not so surprising result given that most of the leisure activities are concentrated in that part of the city. In the case of the population with inactive socio-professional status, the hotspots seem to be concentrated in the northern part of the city, a region known for suffering a thriving inequality.

REFERENCES

[1]Moran PA. The interpretation of statistical maps. *Journal of the Royal Statistical Society. Series B (Methodological)* **10** (1948) 243–251.

[2]Bassolas A, Nicosia V. First-passage times to quantify and compare structural correlations and heterogeneity in complex systems. *Communications Physics* **4** (2021) 1–14.

[3]Bassolas A, Sousa S, Nicosia V. Diffusion segregation and the disproportionate incidence of covid-19 in african american communities. *Journal of the Royal Society Interface* **18** (2021) 20200961.

[4]Lecomte C, Vallée J, Le Roux G, Commenges H. Le mobiliscope, un outil de géovisualisation des rythmes quotidiens des métropoles. *Mappemonde. Revue trimestrielle sur l'image géographique et les formes du territoire* (2018).

[5][Dataset] Vallée J, Douet A, Villard E, Lecomte C, Le Roux G. Mobiliscope (2021). doi:10.5281/zenodo.4670766.

[6]Vallée J, Lenormand M. Intersectional approach of everyday geography. *arXiv* (2021) arXiv:2106.15492.

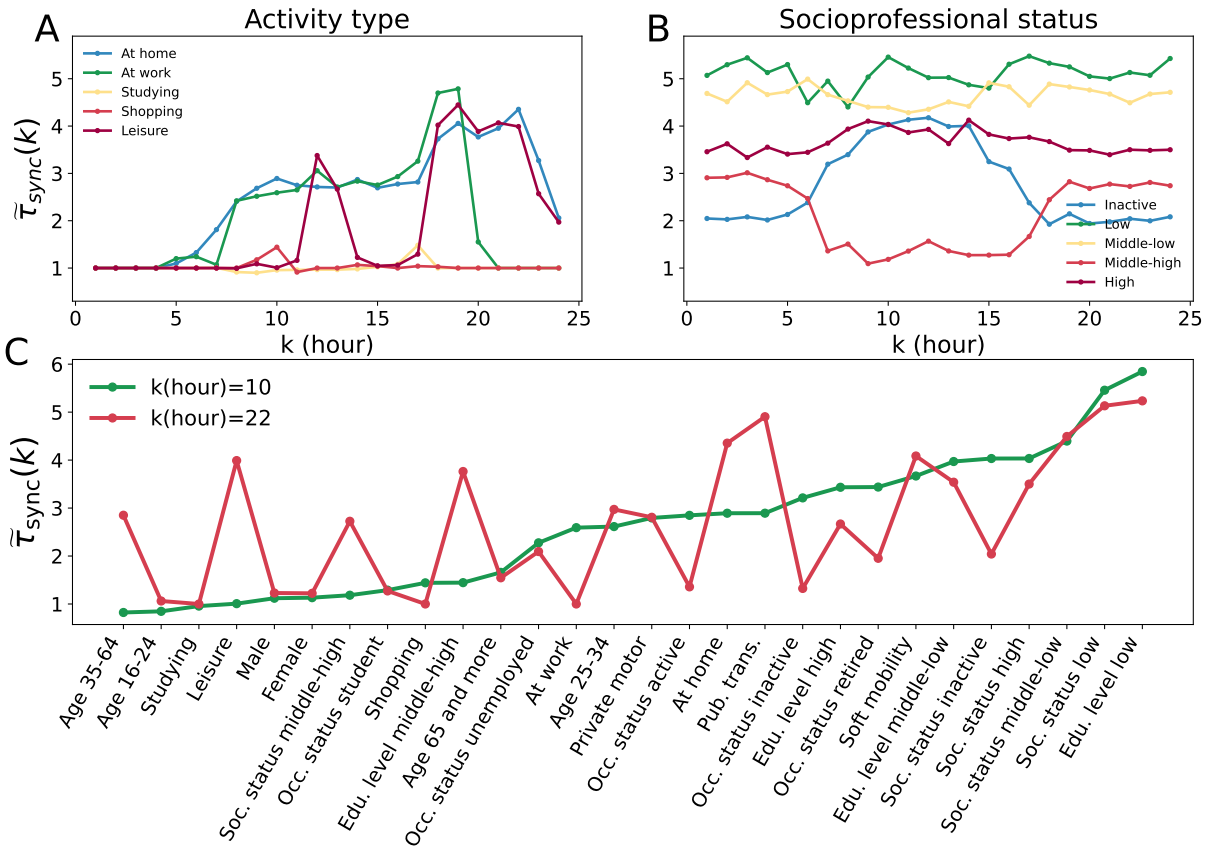

Figure S8. Synchronization around the clock in Paris. (A) Normalized synchronization time for the distribution of population performing each of the five types of activities. (B) Synchronization time for the distribution of population of each socio-professional status. (C) Change of synchronization times for all of the indicators at 10am (green) and 10pm (red).

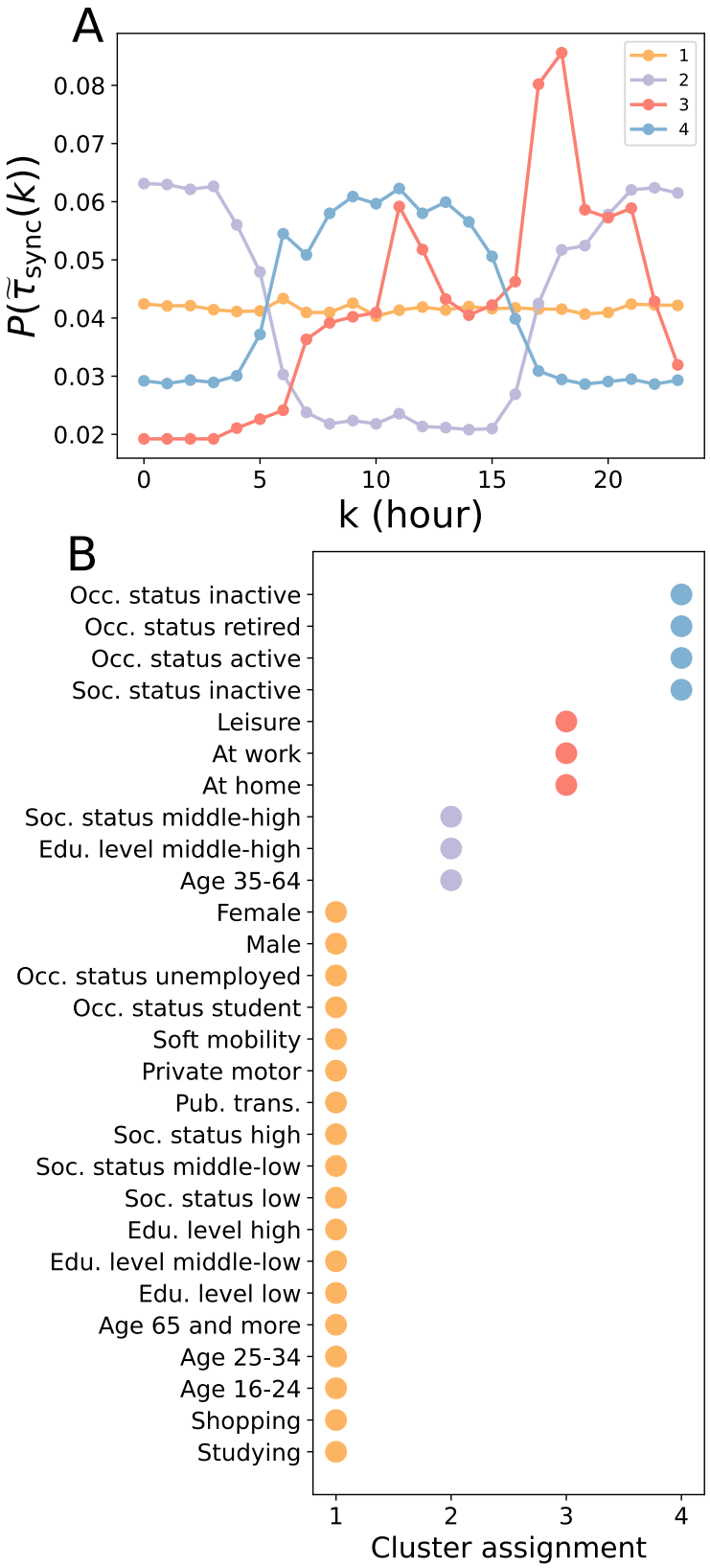

Figure S9. Clustering analysis of segregation around the clock in Paris. (A) Pattern of synchronization times P for each of the four main groups detected with the K-Means algorithm. (B) Cluster assignment for each of the indicators analyzed.

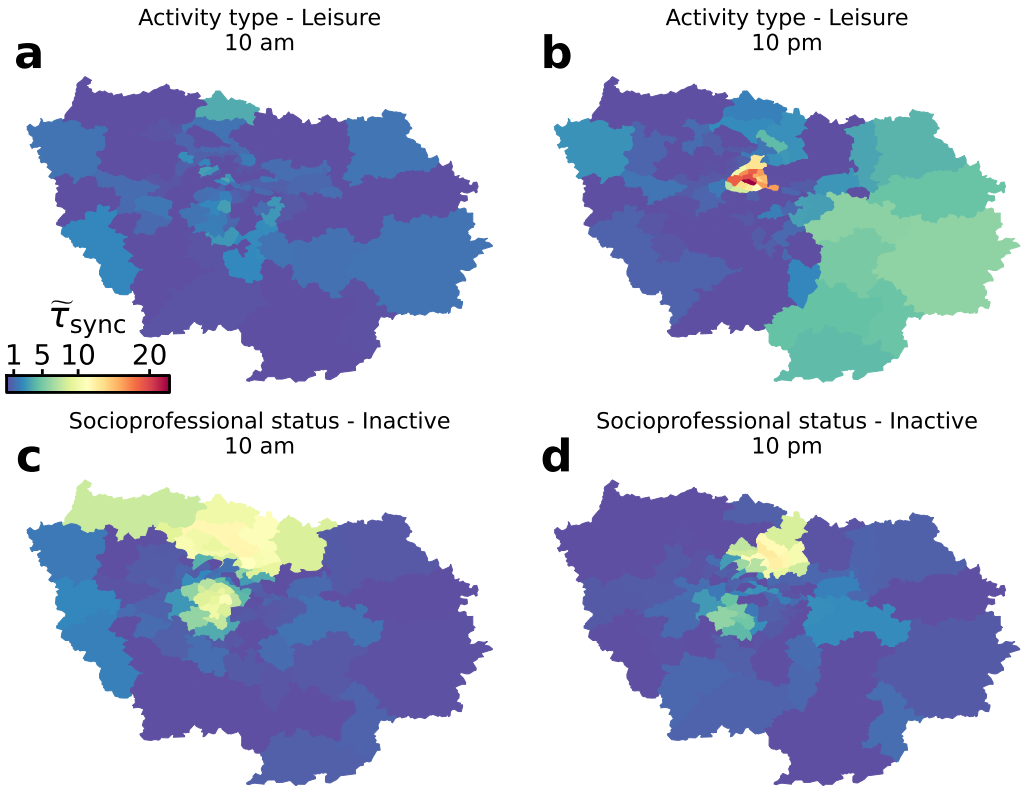

Figure S10. Local synchronization around the clock in Paris. (A, B) Normalized synchronization time for each Paris district for the population performing leisure activities at 10am and 10pm. (C, D) Normalized synchronization time for each Paris district for the population with inactive socio-professional status at 10am and 10pm. For visualization purposes the color range is common to all four maps.